Version 1/28.06.2012

Post-irradiation Electrical Characterisation of MCMD sensors

Technical Note by A.Chilingarov, Lancaster University

Introduction

The measurements were performed with 4 sensors from wafer 9 (BCB thickness 12 μm) irradiated by 26 MeV protons to 1 MeV neutron equivalent fluences from 10^{13} to 10^{16} cm^{-2}. The sensors installed in test frames were tested inside a special box flushed with dry Nitrogen. The box was cooled by Peltier elements. The minimum temperature achievable in the set-up is -32^{o}C. Negative bias voltage was applied to the sensor backside. The absolute value of this voltage is used everywhere in the text below. Maximum voltage allowed in the set-up is 1000V. The bias rail connected to all strips via built-in bias resistors was grounded. The sensor names, their mesh type, irradiation fluence and ionisation dose are summarised in Table 1.

Table 1. Sensors and their irradiation

Sensor #	Sensor name	Mesh type	1 MeV neq./cm^2	Dose, Mrad
1	x2y4	50% - 30μm	10^{13}	1.4
2	x4y1	50% - 80μm	10^{14}	14
3	x5y2	25% - 30μm	10^{15}	140
4	x0y1	50% - 30μm	10^{16}	1400

1. CV and IV measurements

The current through the central part of a sensor, I_c, was calculated as a difference between the total sensor current, I_t, measured at the output of the biasing source-measure unit and the current through the innermost guard ring grounded via an ammeter. The capacitance was measured between the backside and the bias rail in C_s-R_s mode. The bias was ramped up to its maximum value and at each bias point measured were the currents I_t, I_c and the values of C_s and R_s at 4 frequencies: 1, 3, 10 and 30 kHz. Typically the measurements

were made at a temperature close to -20°C. Heavily irradiated sensors #3 and #4 were also measured at -32°C to reduce the effects related to the sensor self-heating.

Some CV and IV curves are shown in Fig.1. For sensors #1 and #2 the measurement temperature was close to -20°C while for sensor #3 it was about -32°C. The capacitance presented in this plot is at 3 kHz frequency for the measurements at -20°C and at 1 kHz for the -32°C data. The values of the central current, I_c, in the plot are corrected to exactly -20°C temperature and scaled to simplify the comparison: the currents in nA are divided by factors 10, 100 and 1000 for sensors ##1, 2 and 3 respectively.

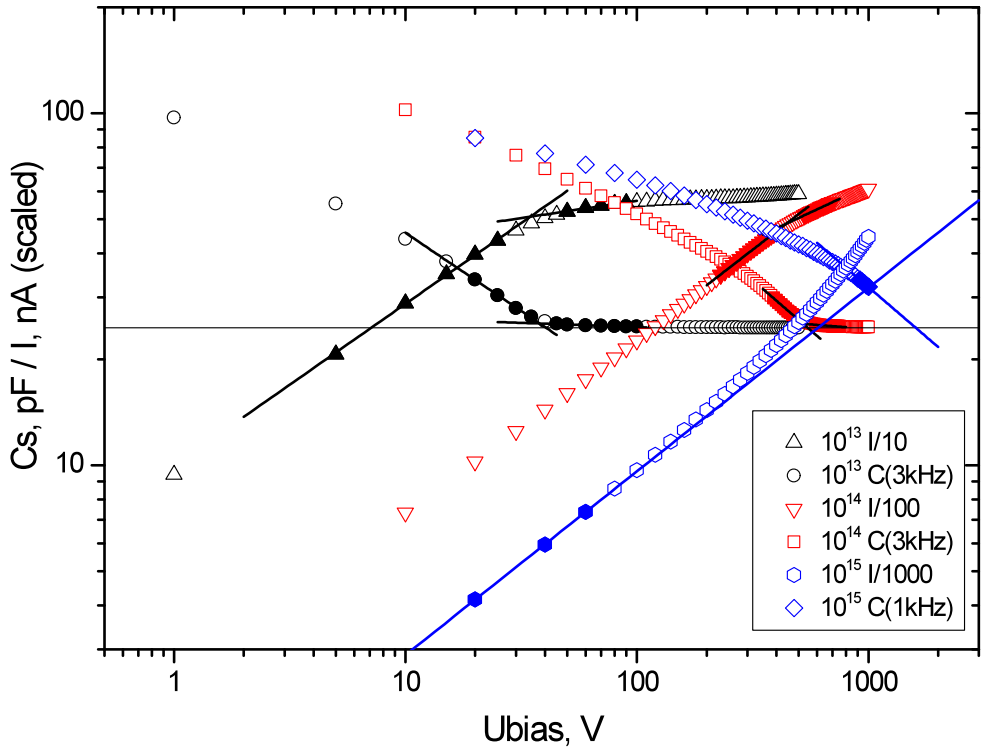

Fig.1. CV and IV curves for sensors ## 1-3. The currents in nA are corrected to -20°C and scaled to simplify the comparison. Where possible the depletion voltage was found from crossing of two straight lines. See text for further details.

The curves for sensors #1 and #2 exhibit a sharp change of the slope – a "kink". For each of these curves the fits of two straight lines (in log-log plots) were made around the kink

positions. These lines are also included in Fig.1. The points used for the fits are shown by filled symbols. The position of the kink vertex (crossing point of the fit lines) along *x*-axis was taken as the full depletion voltage, V_d, measured by a particular method. The kink position along *y*-axis is considered as capacitance or the current at $U_{bias} = V_d$.

The curves for the sensor #3 show no kink indicating the V_d higher than maximum bias of 1000 V used in the measurements. For those curves the straight line fits were made through the first 3 points of the IV and the last 4 points of the CV curves.

The depletion voltage values for the sensors #1 and #2 are summarised in Fig.2. For sensor #1 the measurements were performed twice near -20^{o}C and once near -1^{o}C while for sensor #2 they were made 5 times near -20^{o}C, once near -10^{o}C and once near -28^{o}C. Depletion voltage found from CV curves for those sensors before irradiation are also shown in Fig.2. The latter measurements were made during pre-irradiation sensor characterisation at the Probe Station at a temperature near +20^{o}C and the frequencies of 1, 10 and 20 kHz.

The points show the results obtained from CV data plotted versus measurement frequency. If more than one measurement was made at a given temperature the corresponding point represents the average for those runs. The lines connecting the points are to guide the eye only. In heavily irradiated Si sensors the depletion voltage obtained from CV measurements is known to depend on frequency and temperature [1]. This dependence can be seen in Fig.2 for irradiated sensors. As expected no frequency dependence was observed for non-irradiated sensors. The depletion voltage obtained from the I-V measurements is shown by dashed lines. For each sensor the lower line represents the minimum and upper line the maximum V_d obtained for this sensor in all runs at all temperatures. An overall conclusion from the results presented in Fig.2 is that for sensor #1 irradiated by fluence of 10^{13}cm^{-2} the depletion voltage is ~35V close to the value observed before irradiation, while for sensor #2 irradiated by fluence of 10^{14}cm^{-2} the depletion voltage is ~500V.

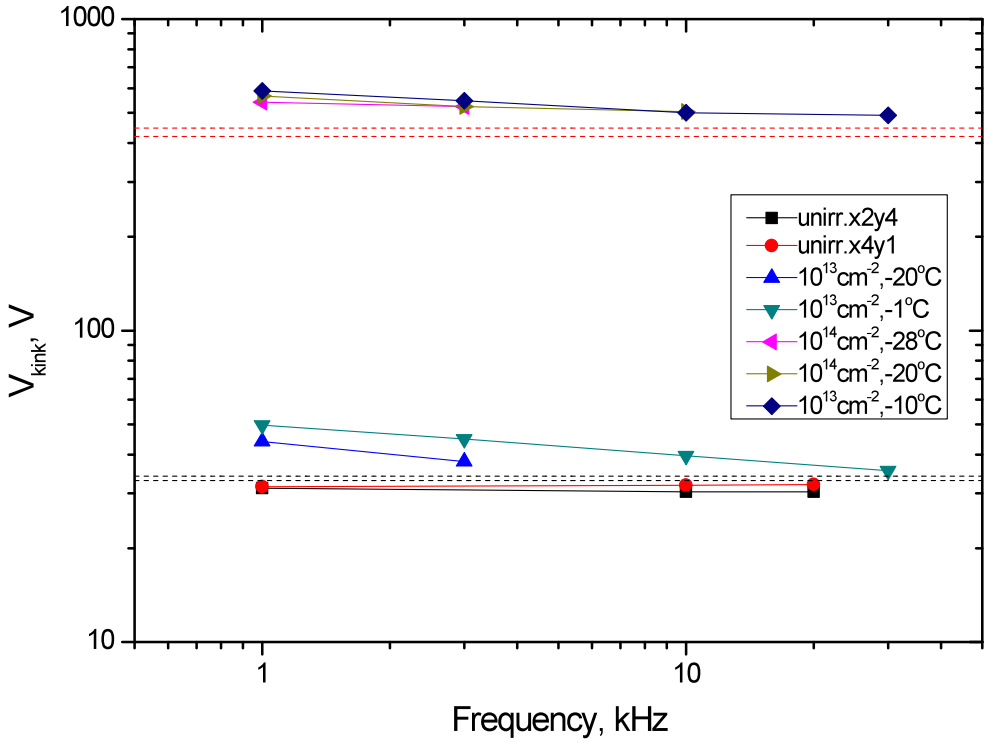

Fig.2. Depletion voltage found from CV and IV measurements. The points correspond to CV results before and after irradiation vs. measurement frequency. The dashed lines are the results from IV measurements after irradiation. See text for further details.

The depletion voltage for sensor #3 can be estimated as follows. From the CV data for sensors #1 and #2 the capacitance at full depletion was found to be 24.6 pF. This value is shown in Fig.1 by a horizontal line. The CV curve for sensor #3 was fit by a straight line through 4 points at highest bias. This line reaches the depletion capacitance value at ~1600V. The IV curve for sensor #3 shows a steady increase in the gradient with bias indicating self-heating of the sensor. The straight line was fit through 3 points of this curve at lowest bias where the self-heating is minimal. The line was extrapolated to the values expected for this sensor at full depletion assuming linear rise of the current with fluence (taken into account by the current normalisation). As can be seen from Fig.1 the line reaches the expected level between 2 and 3 kV. More detailed analysis of the IV curves for sensor #3 and also those for sensor #4 is given later. In any case all the above

estimates for sensor #3 are significantly lower than the value of ~5kV following from a naïve scaling of the V_d value, of ~500 V measured for sensor #2.

The same scaling predicts for sensor # 4 the depletion voltage of ~50 kV. Having in mind the maximum possible bias of 1 kV the CV data for this sensor don't allow any depletion voltage estimates. They can be done only from the IV data. The following analysis of the IV curves was performed for all 4 sensors.

The values of the current I_c at (exactly) -20^{o}C in the "kink" points found for the sensors #1 an #2 were used to obtain the dependence of this parameter on fluence, *F*. In this way the full depletion current at this temperature was parameterised as

$$I_c^{FD}(-20^oC) = 4824.8\ nA*(F/10^{14}cm^{-2}) + 29.3\ nA.$$

Neglecting the small offset one obtains the projected values for I_c at full depletion of 48248 nA and 482480 nA for sensors #3 and 4 respectively. Normalising the measured current by the values from the above equation gives the relative depleted thickness. Fig.3 shows the results for all 4 sensors.

The data for sensors #1 and #2 are from -20^{o}C measurements (corrected to exactly -20^{o}C temperature). For sensors #3 and #4 the measurements were made at -20^{o}C and at the lowest achievable in the set-up temperature (depending slightly on the ambient conditions): -32^{o}C for sensor #3 and -33^{o}C for sensor #4. The currents measured at low temperatures were then scaled up to reproduce at low bias values the data for -20^{o}C in the same sensor. All curves for sensors #3 and #4 exhibit a gradual increase in the I_c gradient with bias. It is more pronounced for higher temperature and higher fluence. Most likely this is due to the sensor self heating.

For sensors #1 and #2 the current below V_d grows approximately as $U^{1/2}$ that is expected for the bulk generated current. For sensors #3 and #4 the current at low bias grows as $U^{0.521}$ and as $U^{0.662}$ respectively. This is shown by the straight line fits performed through the points (marked by the filled symbols in Fig.3) of low temperature data. These points should be practically free from the self-heating effects since they agree well with the data

measured at significantly higher temperature. The fits are shown in Fig.3 by solid lines. They predict the following characteristics for sensors #3 and #4 respectively: the relative depleted thickness at 1000V bias of 66% and 37% corresponding to the full depletion voltage of 2.2 kV and 4.5 kV.

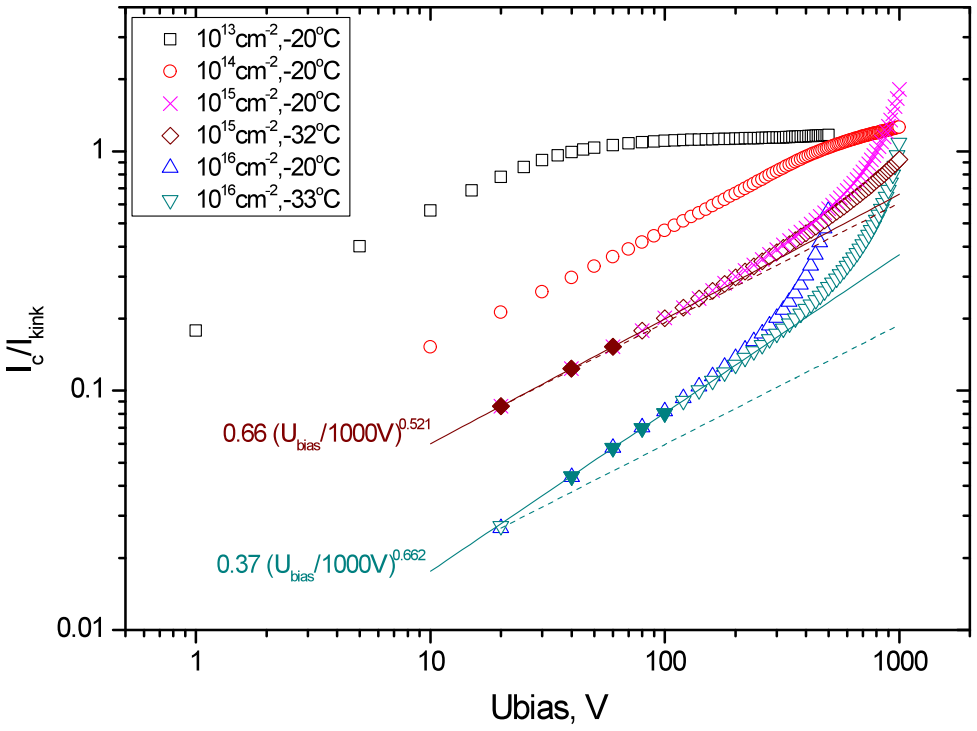

Fig.3. Currents scaled by its values in the kink point for all sensors. The fits through the points shown by filled symbols are presented by solid lines. Scaling of the lowest points for sensors #3 and #4 by the expected dependence of $U^{1/2}$ is shown by dashed lines.

More conservative estimates may be obtained from the scaling of the currents measured at lowest bias points of 20V by the expected $U^{1/2}$ dependence. In this approach the steeper than expected rise is attributed to the sensor self-heating and/or to a contribution from the currents other than those generated in the bulk. This scaling is shown in Fig.3 by dashed lines. In this case the parameters for sensors #3 and #4 are the following: relative depleted thickness at 1000V is 61% and 19% corresponding to the full depletion voltage of 2.7 kV and 28 kV respectively.

Charge collection efficiency (CCE) measurements for these sensors made in Liverpool University gave the following results for 1000 V bias: ~40% for sensor #3 and ~13% for sensor #4. These values do not contradict to the above estimates of relative depleted thickness at 1000 V having in mind the carrier trapping. Systematically lower V_d values compared to the naïve scaling from the results for sensor #2 irradiated by 10^{14} neq/cm^2 may be due to high electric field existing in heavily irradiated sensors across the electrically neutral region (so called "active base" phenomenon) [2].

2. Strip capacitance

As shown in pre-irradiation measurements [3] two major contributions to the capacitive load at the electronics connected to a strip are the interstrip capacitance, C_{is}, and the capacitance between a strip and the ground plane GNDP, C_{sG}. Both these parameters depend on the GNDP type [3]. The irradiated sensors have three GNDP types (see Table 1). The capacitance for un-irradiated sensors with these GNDP types was also measured in the same set-up to simplify the comparison.

a) Interstrip capacitance

The C_{is} measurements were made exactly as in pre-irradiation tests described Ref. [3]. The capacitance was measured between a readout strip and its two immediate neighbours at 6 frequencies from 10 kHz to 1 MHz. The measurement temperature was -20^{o}C for sensors #1 and #2 and -32^{o}C for sensors #3 and #4. Un-irradiated sensors were measured at the same temperature as irradiated ones with the corresponding GNDP type. The capacitance was first measured as a function of bias voltage up to some maximum value, U_{max}, and then as a function of time at this voltage. If the C_{is} changed with time it was allowed to stabilise before the final measurement was taken. For un-irradiated sensors and the one irradiated by 10^{13}cm^{-2} fluence the U_{max} was 500 V. For sensor irradiated by 10^{14}cm^{-2} it was 1000 V and for those irradiated by 10^{15} and 10^{16} cm^{-2} it was 800 V to prevent thermal runaway.

Typical C_{is} value is ~0.8 pF. To measure it with a reasonable precision the contribution from a stray capacitance should be known with very good accuracy. At the Probe Station this problem was solved by making Open Corrections at the LCR meter with all probe needles in correct position but not yet touching the sensor. For sensors mounted in test frames this approach is impossible. Instead the C_{is} offsets were measured for each test frame individually in the whole range of measurement temperatures and subtracted in the analysis. The variations of these offsets due to reconnections of external cables are a major source of uncertainty in reconstructed C_{is} values.

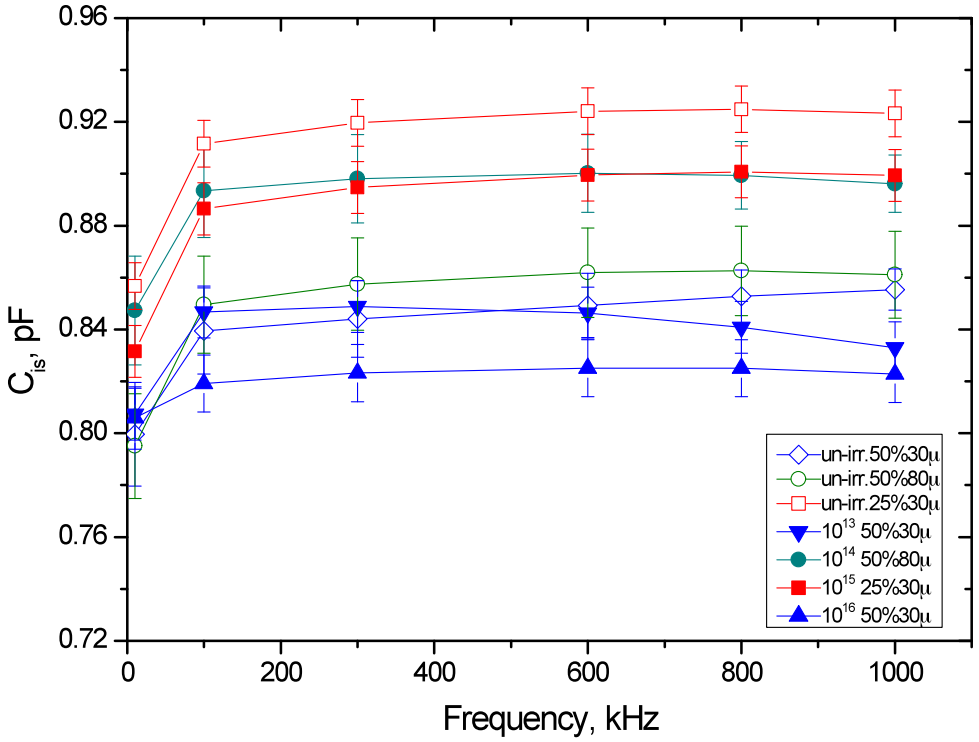

Fig.4. C_{is} at maximum bias vs. measurement frequency for un-irradiated sensors with different GNDP types (open symbols) and the irradiated ones (filled symbols). The lines are to guide the eye. See text for further details.

The C_{is} vs. measurement frequency is shown in Fig.4. Filled points represent the irradiated sensors and open points un-irradiated ones. The GNDP is indicated for all sensors. The lines are to guide the eye. Within uncertainties of ~0.015 pF no effect of

irradiation on C_{is} is observed. With the same accuracy the C_{is} is constant in the frequency range of 100-1000 kHz.

b) Capacitance to GNDP: C_{sG}

As for C_{is} the C_{sG} was first measured as a function of bias and then its stable value was found at maximum bias. The bias values and the measurement temperatures were the same as in C_{is} measurements described above.

A simple way to find C_{sG} is to measure the capacitance from GNDP to the bias rail (to which every strip is connected via bias resistor R_{bias}) and to divide this value by the number of strips covered by GNDP (126 or 128 depending on the GNDP type). This method was used in the pre-irradiation measurements [3]. The capacitance measured in this way will be further referred to as C_{sG}^{plane}. The drawback of the method is that it doesn't work at frequencies above several kHz because of large bias resistor (~2MΩ) connected in series with measured capacitance. For the front-end electronics more relevant is the capacitance at high frequencies. Therefore another method was used to verify that at high frequency the C_{sG} doesn't differ significantly from C_{sG}^{plane}.

The second method is to measure a capacitance between GNDP and connected together several adjacent readout strips. Since for practical reasons the number of such strips, *n*, cannot be large the difficulty of this method is a proper subtraction of the contribution due to the C_{is}. Denote the capacitance measured between *n* strips and GNDP as C_n. It consists of *n* connected in parallel capacitances C_{sG} and two stray capacitances, C_{edge}, from the edge (first and last) strips in the group to GNDP via interstrip capacitive link.

$$C_n = nC_{sG} + 2C_{edge} \qquad (1)$$

Denote capacitance between two adjacent strips as C_{ss}. Then C_{edge} can be written as the capacitance from the edge strip to its nearest neighbour outside the group, C_{ss}, connected in series to C_t – total capacitance of this neighbour strip to GNDP:

$$C_{edge} = \frac{C_{ss}C_t}{C_{ss} + C_t} \qquad (2)$$

Two extreme assumptions can be made about the C_t value: a) $C_t = C_{sG}$, which is the minimum value for C_t, and b) $C_t \to \infty$ that means $C_{edge} = C_{ss}$. Case a) corresponds to the minimum and case b) to the maximum value of C_{edge}. Using measured separately C_{is} and a reasonably safe assumption $C_{ss}=0.5C_{is}$ one can find C_{sG} from eq.(1) for both extreme values of C_t. Clearly the assumption a) results in maximum and assumption b) in minimum value of C_{sG}.

The latter gives very simple expression for C_{sG}:

$$C_{sG} = \frac{C_n - C_{is}}{n} \tag{3}$$

Assumption a) leads to the following equation for C_{sG};

$$nC_{sG}^2 + \left((n+2)C_{ss} - C_n\right)C_{sG} - C_n C_{ss} = 0 \tag{4}$$

Substituting C_{ss} by $0.5C_{is}$, solving equation (4) and leaving only the positive solution for C_{sG} one obtains:

$$C_{sG} = \frac{2C_n - (n+2)C_{is} + \sqrt{\left((n+2)C_{ss} - C_n\right)^2 + 8nC_n C_{is}}}{4n} \tag{5}$$

The C_{sG} was investigated for the same sensors as C_{is}. The C_{sG}^{plane} was measured at frequencies from 1 to 100 kHz and C_n from 10 to 1000 kHz. The latter was measured using the same 3 strips that were used for C_{is} measurements. The average of minimum and maximum C_{sG} values (given by eqs. (3) and (5)) was used as a final result for high frequency method and a half difference between these two values as a measure of its uncertainty. This systematic error is significantly larger than the errors resulting from the C_{is} and C_n measurement uncertainties. The C_{sG} values found by both methods are presented in Fig.5.

The results in the left part of the plot show C_{sG}^{plane}. Above 10 kHz these values quickly decrease with measurement frequency. The results in the right side are from measurement of capacitance between GNDP and 3 readout strips. For three data sets typical systematic errors of this method are shown. At highest frequencies they increase from ~5% for 50% 30μm mesh to ~15 % for 25% 30μm mesh. In all cases the C_{sG} at highest frequency (most relevant) and low frequency (least affected by R_{bias}) agree very well. For sensor

irradiated by 10^{16} cm^{-2} the C_{sG} value is by ~10% higher than for un-irradiated sensor with the same GNDP type. Otherwise no effect of irradiation on C_{sG} is observed.

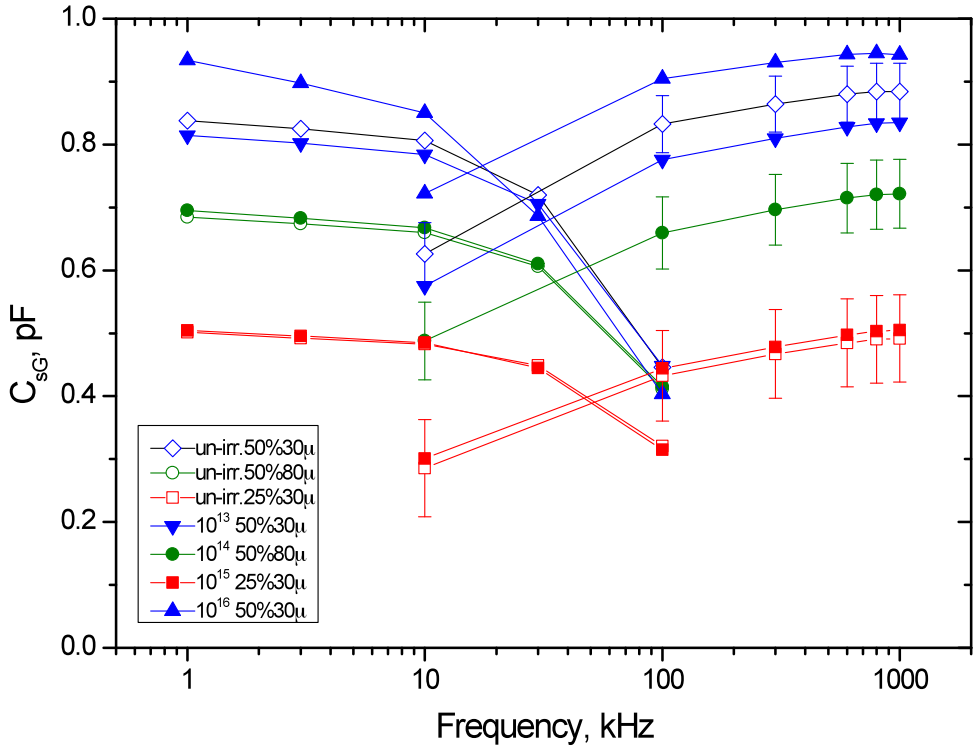

Fig.5. Capacitance between a strip and GNDP for un-irradiated (open symbols) and irradiated sensors (filled symbols). The lines are to guide the eye. Low frequency results are from measurement of capacitance between GNDP and the strip plane; the high frequency ones are from that between GNDP and 3 readout strips. Typical systematic errors for the latter method are shown in 3 cases. See text for further details.

3. Interstrip resistance

Interstrip resistance, R_{is}, was measured in the same way as for un-irradiated sensors described in Ref. [3]. Test DC potential was applied to a strip implant and the voltage induced at the adjacent strip implant was measured. Only every second strip implant was accessible due to layout constrains. As shown in Ref. [4] the maximum measurable R_{is} in this case is ~ 1 GΩ and is limited by non-zero parasitic resistance on the sensor. Before irradiation typical measured R_{is} was ~0.3 GΩ.

For R_{is} measurements in irradiated sensors 3 (accessible) adjacent strips were used. The resistance was measured as a function of bias voltage for two possible pairs of the adjacent strips and the obtained R_{is} values (usually very close) averaged. Measurement temperature was -20°C for sensors #1, #2 and -32°C for sensors #3, #4. The results are shown in Fig.6. In all cases interstrip resistance is much higher than the bias resistors of ~1 MΩ. For all sensors the bias dependence is rather weak. Representative R_{is} values at U_{bias} = 500 V are collected in Table 2.

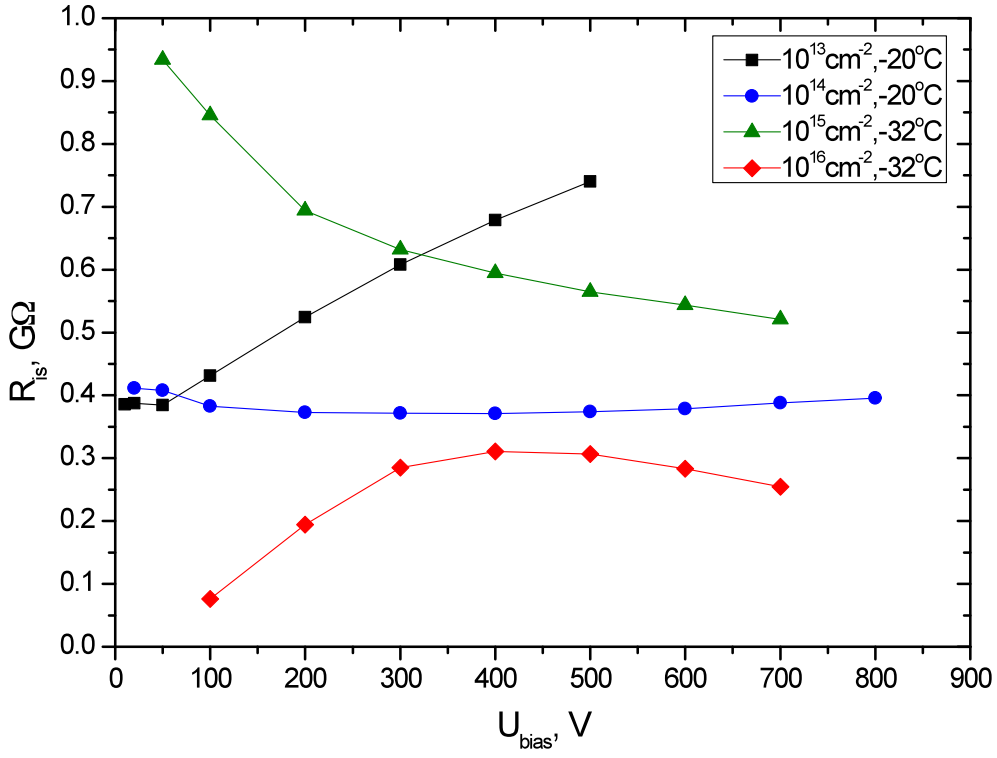

Fig.6. Interstrip resistance for irradiated sensors. Measurement temperature and irradiation fluence are indicated.

4. Punch-through (PT) characteristics

The MCMD sensors were not optimised for efficient punch-through protection (PTP) against a high voltage at the implant strips. The PT develops via 19 μm gap between the

strip implant edge and the bias rail. However for un-irradiated sensors the PTP was found to operate quite successfully. Therefore it's evolution with irradiation is a valuable information.

The PT was measured in the same way as during pre-irradiation characterisation described in Ref. [3]. Negative test potential, V_{strip}, was applied to a strip implant relative to the bias rail and the resulting current was measured. Subtracting from this current the ohmic component V_{strip}/R_{bias} allows finding the PT current. The PT parameters were investigated for each of three strips used for R_{is} measurements. No difference between the strips was observed and the results shown below are for one of them. Measurement temperature was -20^{o}C for un-irradiated sensor and sensors #1, #2 while for sensors #3, #4 it was -32^{o}C. Bias dependence of the PT characteristics is quite weak. Therefore for un-irradiated and the least irradiated sensor the measurements were made at appropriate for them U_{bias} = 300 V while for sensors ## 2-4 at 600 V.

The PT current versus the absolute value of negative voltage applied to the strip is shown in Fig.7. According to literature [5] it should grow first exponentially and then more slowly. This pattern is indeed observed for un-irradiated sensor and that irradiated by 10^{13} cm^{-2}. For more heavily irradiated sensors the dependence becomes quite complicated and contains sharp changes ("jumps"). The latter were reproducible and observed for all 3 investigated strips.

The PT evolution with irradiation can be summarised as follows. The PT onset doesn't change very much. For example the voltage at which the PT current exceeds 10 nA is ~13 V for un-irradiated and the least irradiated sensors while for more heavily irradiated ones it is between 20 and 30V. More significant is a steady decrease with irradiation in the rate of the PT current increase above the onset. Suppose the voltage at the implant should not exceed some safe level, e.g. 50V. In this situation the current that PT can drain from a strip is >100 μA in un-irradiated and the least irradiated sensors while in the sensors irradiated by $\geq 10^{15}$cm^{-2} it is <1 μA. Clearly a dedicated structure is necessary to keep the PTP operational up to such high fluences.

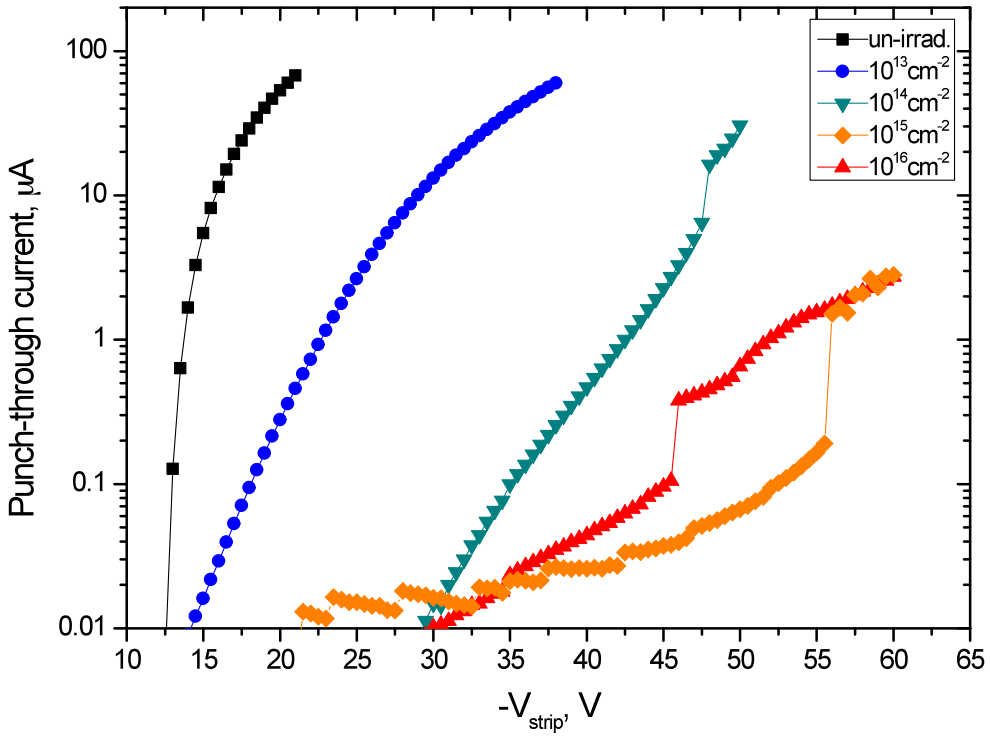

Fig.7. Punch-through current vs. absolute value of negative test voltage for un-irradiated and four irradiated sensors. See text for further details.

Summary

Main sensor parameters after irradiation are summarised in Table.2

Table 2. Main sensor parameters after irradiation.

Sensor #	**Sensor name**	**1 MeV neq. fluence, cm^{-2}**	**V_{dep}**	**C_{is}, pF**	**R_{is} at 500V,GΩ**
1	x2y4	10^{13}	35V	0.833±0.010	0.74
2	x4y1	10^{14}	~500V	0.896±0.011	0.37
3	x5y2	10^{15}	2-3* kV	0.899±0.010	0.56
4	x0y1	10^{16}	5-30* kV	0.823±0.011	0.31

* Estimated

Depletion voltage and the current at it observed for sensor x4y1 were compared with the values following from the study [6] of microstrip detectors made of p-type silicon. They agree within ~20% accuracy. Neither interstrip nor capacitance to the GNDP change with irradiation. Interstrip resistance remains above 100 MΩ up to highest investigated fluence. Simple PT protection in a form of 19 μm gap at the strip edge operates effectively up to the fluence of 10^{13} neq/cm^2 but is much less efficient after higher irradiation.

References

1. D.Campbell, A.Chilingarov and T.Sloan, Nucl.Instr.&Meth. A492 (2002) 402.
2. G.Kramberger et al., IEEE Trans.Nucl.Sci. 57 (2010) 2294.
3. L.Eklund et al., NIM A623 (2010) 162.
4. A.Chilingarov, "Interstrip resistance measurement", CERN PH Note, PH-EP-Tech-Note-2011-01, 21.9.2010.
5. J.Lohstroh et al., Solid-State Electronics, 24 (1981) 805.
6. M.D.L.Hanlon, "The Development of p-type Silicon detectors for the High radiation Regions of the LHC", PhD thesis, Liverpool, 1999.